CERN LHC signals for a neutrino mass model with bilinear R-parity violating minimal anomaly mediated supersymmetry

F. de Campos[*]

Departamento de Física e Química, Universidade Estadual Paulista, Guaratinguetá, SP, Brazil

M. A. Díaz[+]

Departamento de Física, Universidad Católica de Chile, Av. V. Mackenna 4860, Santiago, Chile

O. J. P. Éboli[‡]

Instituto de Física, Universidade de São Paulo, São Paulo, SP, Brazil

M. B. Magro[§]

Faculdade de Engenharia, CUFSA Santo André, Brazil

W. Porod[‖]

Institut für Theoretische Physik and Astrophysik, Universität Würzburg, D-97074 Würzburg, Germany

S. Skadhauge[¶]

Nordita, AlbaNova University Center, Roslagstullbacken 23, SE-10691 Stockholm, Sweden

We investigate a neutrino mass model in which the neutrino data is accounted for by bilinear R-parity violating supersymmetry with anomaly mediated supersymmetry breaking. We focus on the CERN Large Hadron Collider (LHC) phenomenology, studying the reach of generic supersymmetry search channels with leptons, missing energy and jets. A special feature of this model is the existence of long-lived neutralinos and charginos which decay inside the detector leading to detached vertices. We demonstrate that the largest reach is obtained in the displaced vertices channel and that practically all of the reasonable parameter space will be covered with an integrated luminosity of 10 fb^{-1}. We also compare the displaced vertex reaches of the LHC and Tevatron.

I. INTRODUCTION

The neutrino sector is one of the most exciting sectors of particle physics today. Our knowledge of the neutrino parameters has increased tremendously during the past decade. Both the atmospheric and the solar mass squared differences and mixing angles are known to a good precision [1–5]. However, only an upper bound exists on the so-called CHOOZ angle, $\sin^2\theta_{13} < 0.04$ [6], and the absolute mass scale for the neutrino masses, $\sum m_\nu \lesssim 0.6$ eV [7]. Furthermore, there is an ambiguity in the sign of the atmospheric mass square difference leading to the possibility of two different hierarchies, normal or inverse, for the neutrino masses.

As the neutrino experiments enter a precision phase the need to explore different neutrino mass models increases. The most popular model for neutrino masses, the seesaw mechanism [8], beautifully explains the smallness of the neutrino masses as compared to other fermion masses. Nevertheless, it is difficult to test this mechanism due to its very high energy scale. The right-handed neutrinos introduced in the seesaw model have masses of order 10^{12} GeV and are too heavy to be produced in colliders.[1] On the other hand, models where the origin of neutrino masses is related to TeV-scale physics have been proposed [10,11] and these might be tested at the future or even present colliders [12,13].

In this paper we will consider a TeV-scale mechanism for generating neutrino masses, namely, through R-parity violating (RPV) supersymmetry (SUSY) [14]. In this scenario the neutrino and neutralinos mix giving rise to the neutrino masses [15]. We will be constraining ourself to bilinear RPV (BRpV) [16,17], thus breaking lepton number but not baryon number. This model can be viewed as the effective theory of a spontaneously broken R-parity symmetry [18]. The BRpV neutrino mass model has only a few free parameters and therefore is very predictive.

---

[*]camposc@feg.unesp.br
[+]mad@susy.fis.puc.cl
[‡]eboli@fma.if.usp.br
[§]magro@fma.if.usp.br
[‖]porod@physik.uni-wuerzburg.de
[¶]solveig@nordita.org

---

[1]However, one might see there traces in the properties of the left sneutrinos [9].

Furthermore, in contrast to trilinear RPV neutrino mass models, the constraints from LEP on the R-Parity violating couplings are automatically satisfied as the couplings are small.

We will study the specific case of anomaly mediated supersymmetry breaking (AMSB) [19,20]. In this scenario the contribution to the soft-supersymmetry breaking terms from the superconformal anomaly, which is always present, is assumed to be dominant. AMSB naturally solves the flavor problem of the minimal supersymmetric standard model (MSSM), since the masses of the two first generations of scalars are automatically equal and the flavor off-diagonal terms are given in terms of the quark Yukawa couplings. However, anomaly mediation in its pure form is not a viable theory since without any other soft symmetry breaking terms, tachyonic sleptons are present in the particle spectrum. Therefore, one normally adds an universal scalar mass term. This minimal anomaly mediated scenario (mAMSB) is the one we will pursue in an extended form where we also add bilinear R-parity violation.

It has been shown that mAMSB with BRpV can account for the present neutrino data [21,22]. Like any SUSY BRpV neutrino mass model it predicts the normal hierarchy, since the neutrino masses becomes strongly hierarchical. The hierarchy is induced because only one neutrino mass is generated at tree-level and the other masses are generated at loop level. In general the atmospheric mass squared difference and mixing angle are related to tree-level physics, whereas the solar mass squared difference and mixing angle are established by radiative corrections. The introduction of RPV will render the lightest supersymmetric particle (LSP), which in mAMSB is normally the lightest neutralino, unstable. Clearly, this fact will be very important for the collider phenomenology. Indeed, the standard signal with much missing energy expected from R-parity conserving (RPC) supersymmetry will be depleted.

The RPV couplings giving rise to neutrino masses are also responsible for the decay properties of the neutralino. Therefore, an important smoking gun signal for these models is the strong connection between neutralino physics and neutrino mixing parameters. Some ratios of the branching ratios of the neutralino are related to neutrino mixing angles [23,24]. In particular, approximately the same number of muon as taus are expected along with a W-boson because their ratio is given by tangent of the nearly maximal atmospheric mixing angle. By measuring the decay properties of the neutralino, which is likely to be done by the LHC, a severe test of this model is possible.

Because of the smallness of the RPV couplings the neutralino will have a long lifetime, but short enough for it to mainly decay within the detectors at the LHC. A distinct feature of the mAMSB scenario is the near degeneracy of the lightest neutralino and the lightest chargino, causing even the chargino to dominantly decay through RPV couplings. Consequently, also the chargino will have a lifetime in the range interesting for colliders such that it will travel a macroscopic distance but decay before leaving the inner detector. A very interesting and unique signal will therefore be the observation of displaced vertices from the neutralino and the chargino. Displaced vertices may also be produced, although only arising from neutralino, in the minimal supergravity (mSUGRA) scenario and has been shown to give an excellent reach of the model parameters [25]. As the mAMSB has two different long-lived sparticles, there is a richer set of possible final states.

The prospects for collider discovery of RPV, responsible for the neutrino masses and mixings, in mSUGRA have been thoroughly studied [23–27]. Also, the discovery prospects for mAMSB with R-parity conservation at colliders have been analyzed [28–30]. Nevertheless, the collider signals within R-parity violating mAMSB scenario have been analyzed so far only considering trilinear R-parity violation [31]. In this paper we will study the BRpV-mAMSB scenario, requiring that the neutrino masses and mixings are generated by the RPV couplings. We will analyze various generic SUSY search channels for the LHC. In addition we will also determine the reach in the displaced vertices channel.

We organize the paper as follows. In Sec. II we will review the model and the main low energy constraints. In Sec. III we outline our choice of final state channels and describe our simulation of the signals and backgrounds. In Sec. IV we present our results, as well as, our conclusions.

II. ANOMALY MEDIATED SUPERSYMMETRY WITH BRPV

In this section we will give a short review of the model we analyze. For further details we refer to [22]. The R-parity conserving soft terms will be assigned according to the minimal anomaly mediated scenario. In addition we will allow for bilinear R-parity violation which contributes in total with six more parameters. The R-parity violating couplings are restricted to values which are consistent with the neutrino data, which severely constraints the available parameter space.

Let us start by describing the mAMSB model. This model can be parametrized by three parameters and a sign,

$$m_{3/2}, \quad m_0, \quad \tan\beta, \quad \text{sign}(\mu) \tag{1}$$

all defined at the high energy scale M_{GUT}. The gravitino mass, $m_{3/2}$, is much larger than the other masses, as this is the only one generated at tree level. All the soft breaking terms are proportional to the gravitino mass in pure AMSB. However, as mentioned above, in order to avoid tachyonic slepton masses an extra universal scalar mass m_0^2 is added to all sfermions and Higgs masses in mAMSB. The ratio between the vacuum expectation values of H_u and H_d is as usual denoted by $\tan\beta$. Finally, the sign of the Higgs/

Higgsino mixing parameter, μ, is free. Our conventions are such that μ enters the superpotential as $-\mu\hat{H}_d\hat{H}_u$. For the explicit relations between the input parameters in (1) and the soft breaking terms in mAMSB see e.g. [32].

A typical spectrum for the anomaly mediated scenario is shown in Fig. 1. Throughout most of the viable parameter space the lightest neutralino is the LSP, with only a small area having the stau or the tau-sneutrino as the LSP. Whether the stau is heavier or lighter than the tau*sneutrino depends on the value of $\tan\beta$. For sufficient high values of m_0 the lightest neutralino will be the LSP. The gaugino masses are proportional to their beta functions, resulting in the unique relationship for AMSB: $M_1:M_2:M_3 \sim 3:1:7$. Here M_i are the gaugino masses; M_1 is the bino mass, M_2 the wino mass and M_3 the gluino mass. This explains the first of two distinct characteristics of the mAMSB spectrum; the near degeneracy of the lightest neutralino (also the LSP is most cases) and the lightest chargino. As the wino mass is much lighter than the others it will be almost equal to the masses of the lightest states, with the neutral state being slightly lighter. The winolike nature of the lightest neutralino is important as its interactions are stronger and it will be more easily produced at colliders. The second characteristic, the near degeneracy of the sleptons, is a less robust feature, as it is a consequence of the assumption of a universal extra contribution to the scalar masses and thus a feature of the minimal AMSB.

The invariance under R-parity, defined by $R_p = (-1)^{3(B-L)+2S}$, is normally assumed in supersymmetric models. This is mainly motivated by two requirements: to obtain a stable proton and to get the LSP as a dark matter

candidate. However, the first requirement can also be obtained by different symmetries forbidding only baryon number violating terms; see, e.g., [33]. Introducing lepton number violating terms has the benefit that neutrino masses are generated in an intrinsically supersymmetric way. We will introduce bilinear R-parity violation in order to produce the observed neutrino masses and mixings. Thus, we add the following term

$$W_{\mathrm{BR}pV} = \epsilon_i\hat{L}_i\hat{H}_u, \qquad i = 1, \ldots, 3 \qquad (2)$$

to the MSSM superpotential. In order to acquire agreement with the neutrino data, the R-parity violating couplings must satisfies $\epsilon_i \ll \mu$. For consistency also the soft breaking terms,

$$B_i\epsilon_i L_i H_u, \qquad i = 1, \ldots, 3 \qquad (3)$$

are added to the MSSM. Thus, six parameters related to break down of R-parity invariance are introduced. In general this will give rise to sneutrino vacuum expectation values (vevs), which in turn leads to mixing between neutralinos and neutrinos. The four heaviest states from the diagonalization of the 7×7 neutralino-neutrino mass matrix will be almost pure neutralino states and we denote these by χ_k^0, $k = 1, \ldots, 4$. Moreover, we arrange them in order of magnitude of the masses, thus, χ_1^0 is the lightest neutralino. The chargino-charged lepton mass matrix is treated in an analog way and the lightest chargino is denoted by χ_1^+.

Clearly the introduction of RPV has important consequences for the collider phenomenology as it will render the LSP unstable. As mentioned above, the lightest supersymmetric particle is normally the lightest neutralino in mAMSB as is the case in mSUGRA. As we allow for R-parity violation, also the areas with stau or sneutrino LSP are viable, these particles will decay. Nevertheless, since the stau or sneutrino LSP parameter space regions are very small, we will not discuss these areas further although they are properly included in our analysis. In the following discussion we will assume that χ_1^0 is indeed the LSP.

As mentioned above, the R-parity conserving parameters are calculated as in the mAMSB scenario. Thus, these are fixed at the scale M_{GUT} and renormalization group equation (RGE) running is used in order to extract the low energy parameters. We will use the program SPheno [34], suitably expanded to the case of RPV, for calculating the mass spectrum and decay widths. For the RPC parameters we use 2-loop RGE's and we include all 1-loop threshold corrections. The unification scale is defined as the scale where the $U(1)$ and the $SU(2)$ coupling constants meet. The RPV couplings are only dealt with at the low energy scale. In the case of the bilinear parameters in the superpotential this can be done consistently without any additional assumption as also the modulus of μ is calculated at the electroweak scale and the bilinear parameters form a closed system within the RGE evolution [35]. The corre-
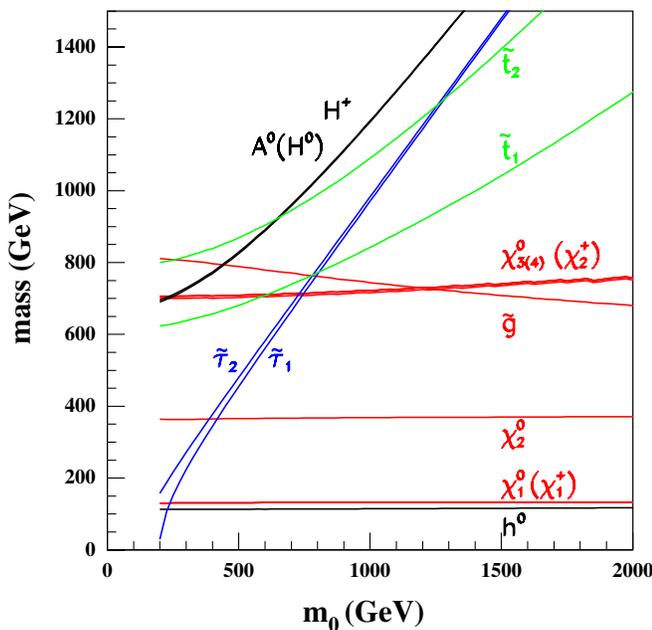

FIG. 1 (color online). Various sparticle masses for $\tan\beta = 10$, $\mu > 0$, and $m_{3/2} = 40$ TeV as a function of m_0.

sponding soft SUSY breaking parameters also form a closed system [35] but one has to assume that there are additional contributions at the high scale similar to the case of the scalar mass parameters squared to get a consistent picture.

The parameters of Eqs. (2) and (3) are determined with the help of neutrino physics. First we trade the B_i by the sneutrino vevs v_i using the tadpole equations. The neutrino masses and mixings are best parametrized using the quantities $\Lambda_i = \mu v_i + \epsilon_i v_d$ and $\tilde{\epsilon}_i = V_{ij}\epsilon_j$ where V_{ij} is the mixing matrix of the tree-level neutrino mass matrix [17]. In case the tree-level contribution dominates in the effective neutrino mass matrix, the modulus of $\vec{\Lambda}$ is fixed by requiring the correct atmospheric neutrino mass difference squared, the atmospheric neutrino mixing angle, and the Chooz angle within the allowed experimental range. In addition, the ratios $|\vec{\epsilon}|^2/|\vec{\Lambda}|$ and $\tilde{\epsilon}_1/\tilde{\epsilon}_2$ are fixed by requiring the correct solar mass difference and solar mixing angle within the experimental range, respectively.

The very particular near degeneracy of χ_1^0 and χ_1^+ is preserved in our model, as the R-parity violating couplings have little impact on the sparticle masses. It is important to calculate the chargino and neutralino masses very precisely, as the mass splitting between these particles, $\Delta m_\chi = m_{\chi_1^0} - m_{\chi_1^+}$, is very small and the exact value can have important consequences for the chargino lifetime. In our numerical evaluation, the neutrinoï-neutralino and chargino-charged-lepton mass matrices are evaluated to 1-loop order.

A. Constraints on the model

Here we will discuss the existing constraints from low energy observables. Besides the requirement of agreement with neutrino data, there are also important constraints from the LEP data, the rare process $b \to s\gamma$ and the anomalous magnetic moment of the muon.

We use the following neutrino constraints, which are the present ones at 90% confidence level:

$$+ 7.3 \times 10^{-5} \text{ eV}^2 < \Delta m_{\text{sol}}^2 < +9.0 \times 10^{-5} \text{ eV}^2$$
$$0.25 < \sin^2\theta_{\text{sol}} < 0.37 \tag{4}$$

$$1.5 \times 10^{-3} \text{ eV}^2 < |\Delta m_{\text{atm}}^2| < 3.4 \times 10^{-3} \text{ eV}^2$$
$$0.36 < \sin^2\theta_{\text{atm}} \le 0.64. \tag{5}$$

It is not always possible to succeed in generating the observed neutrino masses and mixings, and such points will be excluded from our analysis.

The LEP collider at CERN has already put lower bounds on some of the supersymmetric sparticle masses. We have implemented the following constraints from LEP [36]:

$$m_{\tilde{t}} > 95 \text{ GeV}, \qquad m_{\tilde{b}} > 85 \text{ GeV}, \qquad m_{\tilde{\tau}} > 79 \text{ GeV},$$
$$m_{\tilde{\chi}^+} > 95 \text{ GeV}, \qquad m_{\tilde{\chi}^0} > 42 \text{ GeV}, \qquad m_{h^0} > 95 \text{ GeV}. \tag{6}$$

We have checked that also the Tevatron bounds on squark and gluino masses are satisfied [37]. The limit on the Higgs mass is somewhat optimistic as the bound in the MSSM is the same as for the SM Higgs throughout most the available parameter space.[2] For this reason we exhibits the contour for $m_{h^0} = 114$ GeV in our plots of the collider reach. The lower bound on the chargino mass translates almost directly to a lower bound on $m_{3/2}$. For $\tan\beta = 10$ we must require $m_{3/2} > 30$ TeV in order to satisfy the chargino mass bound.

The value of the supersymmetric contribution (δa_μ) to the magnetic moment of the muon is shown in Fig. 2 for $\tan\beta = 10$. The most recent data shows a 3.4σ disagreement with the standard model (SM) value, having $\delta a_\mu = (27.6 \pm 8.1) \times 10^{-10}$ [39]. As is well known the sign of δa_μ tracks the sign of the μ-parameter, in theories where the wino and the bino mass are positive. Therefore, clearly the case $\mu < 0$ is disfavored.

The value of BR($b \to s\gamma$) is shown in Fig. 3 for $\tan\beta = 10$. The current experimental value reads, BR($b \to s\gamma$) = $(3.55 \pm 0.26) \times 10^{-4}$, which is in fine agreement with the standard model expectations. The supersymmetric contribution to this rare process is enhanced by $\tan\beta$ [40] and in general the rate only deviates from the standard model value for large $\tan\beta$. Therefore, the whole region in Fig. 3 lies within the 3σ range. Please note that as the gluino mass is negative in anomaly mediated supersymmetry one does not find a preference for $\mu > 0$ as in the mSUGRA scenario.

For large values of $\tan\beta$ (about 40) and $\mu > 0$ the neutrino data cannot be fitted for low values of m_0. Moreover, for large $\tan\beta$ the bound on the lightest neutral Higgs, as well as the rate of $b \to s\gamma$, rules out a large corner of the low m_0 and low $m_{3/2}$ parameter space. Furthermore, for $\mu < 0$ the constraints from $g - 2$ of the muon excludes all of the parameter-space at 3σ for $\tan\beta = 10$. As the supersymmetric contribution to the magnetic moment of the muon is proportional to $\tan\beta$, the disagreement with the measured values only becomes worse at large $\tan\beta$. Henceforth, we will focus our analysis at a relative low value of $\tan\beta$, which we fix to be 10, and assume that μ is positive.

B. Neutrino parameters

In this section we study a case solution for neutrino physics within the context of BRpV-mAMSB. We concentrate in the following point of mAMSB parameter space,

---

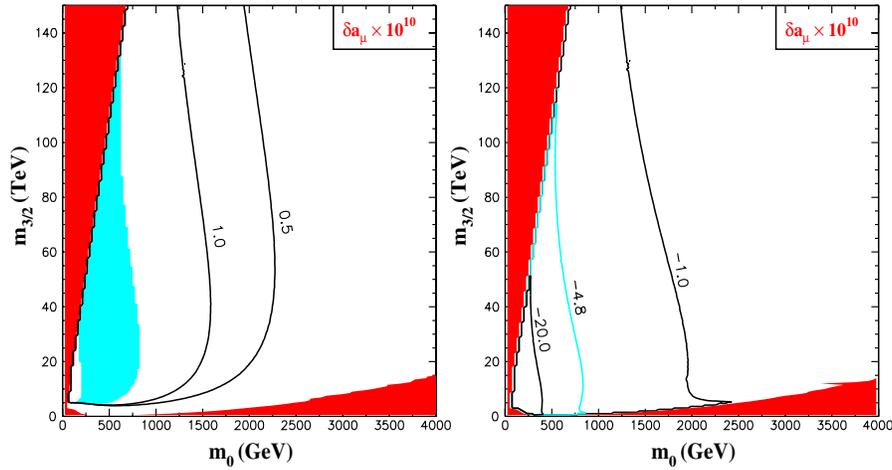[2]Only for small pseudo scalar mass can a lighter Higgs boson be permitted [38].

FIG. 2 (color online).   The supersymmetric contribution to the anomalous magnetic moment of the muon for $\tan\beta = 10$ and $\mu > 0$ (left), $\mu < 0$ (right panel). The dark (red) area is theoretically excluded, due to either tachyonic particles or the fact that the electroweak symmetry is not broken. The light (cyan) area in the left panel is the allowed 3σ range. We also show the contour for $\delta a_\mu = -4.8 \times 10^{-10}$ in the right panel, which corresponds to the 4σ lower bound.

$$m_{3/2} = 40 \text{ TeV}, \qquad m_0 = 500 \text{ GeV},$$
$$\tan\beta = 10, \qquad \mu > 0 \tag{7}$$

which leads to reasonable values for $B(b \rightarrow s\gamma)$ and δa_μ, as can be seen from Figs. 2 and 3. In the spectrum of this model, the Higgs sector is characterized by a light Higgs mass of $m_h = 111.4$ GeV and a relatively heavy charged Higgs with $m_{H^\pm} = 834$ GeV. The LSP is the first neutralino with $m_{\chi_1^0} = 120.85$ GeV, followed by a nearly degenerate chargino with $m_{\chi_1^+} = 120.88$ GeV. The lightest slepton is the stau with $m_{\tau_1} = 458$ GeV, and the lightest squark is the stop with $m_{t_1} = 672$ GeV.

The main effect in collider physics of the presence of BRpV is the instability of the neutralino. But in addition, in the neutrino sector we gain a mechanism for generating masses for the neutrinos, which in turn explain their oscillations. An example solution for neutrino physics, which

we call benchmark 1, is given by the following BRpV parameters,

$$\epsilon_1 = -0.0117, \qquad \epsilon_2 = -0.43,$$
$$\epsilon_3 = -0.246 \text{ GeV} \qquad \Lambda_1 = -0.0467, \tag{8}$$
$$\Lambda_2 = 0.00305, \qquad \Lambda_3 = 0.0689 \text{ GeV}^2.$$

It predicts the following neutrino observables,

$$\Delta m_{\text{atm}}^2 = 2.4 \times 10^{-3} \text{ eV}^2, \qquad \Delta m_{\text{sol}}^2 = 8.0 \times 10^{-5} \text{ eV}^2,$$
$$\tan^2\theta_{\text{atm}} = 1.27, \qquad \tan^2\theta_{\text{sol}} = 0.49, \qquad \tan^2\theta_{\text{reac}} = 0.027. \tag{9}$$

These results are calculated from the full one-loop renormalized 7×7 neutralino-neutrino mass matrix.

In order to gain some insight into the problem, we study next some approximations. It is known that for small
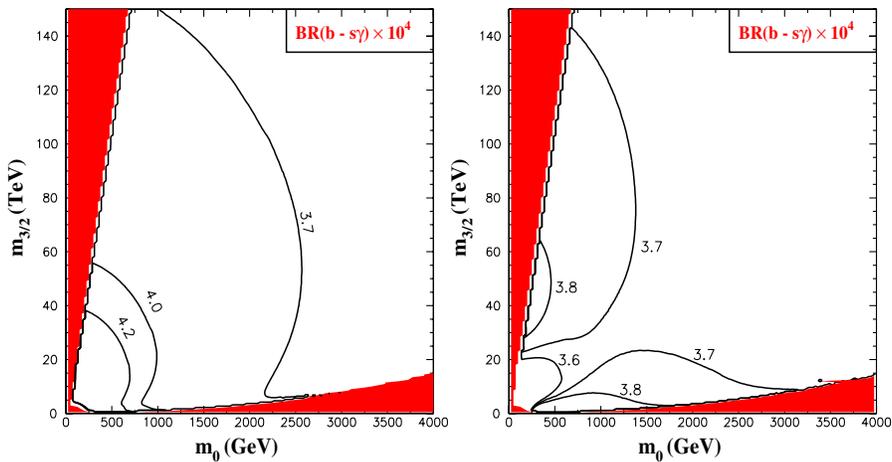

FIG. 3 (color online).   The rate of $b \rightarrow s\gamma$ for $\tan\beta = 10$ and $\mu > 0$ (left), $\mu < 0$ (right panel).

BRpV parameters, the 3×3 effective neutrino mass matrix takes the form,

$$M_{ij}^{\nu} = A\Lambda_i\Lambda_j + B(\Lambda_i\epsilon_j + \Lambda_j\epsilon_i) + C\epsilon_i\epsilon_j \qquad (10)$$

where A receives contributions from tree level as well as one-loop, and B and C are one-loop generated. These three parameters depend only on MSSM masses and couplings and not on BRpV parameters. All the dependence on BRpV is in the ϵ_i and Λ_i. From the 7×7 mass matrix in benchmark 1, the corresponding numerical values for the A, B, and C parameters of the 3×3 effective mass matrix are,

$$A \approx -2.10 \text{ eV/GeV}^4, \qquad B \approx 0.157 \text{ eV/GeV}^3,$$
$$C \approx -0.162 \text{ eV/GeV}^2. \qquad (11)$$

The error we make when we use the approximation in Eq. (10) can be estimated with a χ^2 evaluated at the input values given in Eq. (8), where we defined χ^2 as

$$\chi^2 = \left(\frac{\Delta m_{\text{atm}}^2 - 2.35}{0.95}\right)^2 + \left(\frac{\Delta m_{\text{sol}}^2 - 8.15}{0.95}\right)^2$$
$$+ \left(\frac{\sin^2\theta_{\text{atm}} - 0.51}{0.17}\right)^2 + \left(\frac{\sin^2\theta_{\text{sol}} - 0.305}{0.075}\right)^2 \qquad (12)$$

where the central values and 3σ deviations were taken from Ref. [41]. The atmospheric mass difference is given in 10^{-3} eV^2, and the solar mass difference in 10^{-5} eV^2. Both are defined to be positive. The neutrino observables calculated with the effective 3×3 mass matrix give the value $\chi^2 = 5.7$, most of it coming from the solar angle, indicating the kind of error we make when we use it.

For illustrative purposes, we find now the least modified values of BRpV parameters that give a good solution for neutrino observables calculated using the diagonalization of the effective 3×3 neutrino mass matrix in Eq. (10). We call it benchmark 1':

$$\epsilon_1 = -0.0117, \qquad \epsilon_2 = -0.50, \qquad \epsilon_3 = -0.16 \text{ GeV},$$
$$\Lambda_1 = -0.064, \qquad \Lambda_2 = 0.00305, \qquad \Lambda_3 = 0.033 \text{ GeV}^2. \qquad (13)$$

The difference between this benchmark 1' and the one in Eq. (8) indicates us how erred would be the determination of BRpV parameters if we do not use the full 7×7 mass matrix in the calculation of the neutrino observables.

In Fig. 4 we plot χ^2, which measures the deviation of a given model prediction from the experimental measurements. We calculate χ^2 using the 3×3 effective mass matrix, and we use benchmark 1'. In the left frame we vary ϵ_2 and ϵ_3, keeping all the other parameters constant as indicated by benchmark 1'. In the right frame we vary Λ_1 and Λ_3. By construction, the minimum appear at the values defined by benchmark 1'. The fact that small deviations on the BRpV parameters produce very large values of χ^2 indicate us how sensible are the neutrino observables to them.

To explore in more detail the dependence of each neutrino observable on BRpV parameters we define the quantities χ_i^2, $i = 1, 4$ as the χ^2 calculated using only the ith term in Eq. (12). As in Fig. 4, the χ_i^2 are calculated using the 3×3 effective neutrino mass matrix approximation. We start with atmospheric parameters in Fig. 5. In the left frame we have χ_1^2,

$$\chi_1^2 = \left(\frac{\Delta m_{\text{atm}}^2 - 2.35}{0.95}\right)^2 \qquad (14)$$

which is no more than the first term in Eq. (12), associated with the atmospheric mass squared difference, plotted as a function of ϵ_2 and ϵ_3. In the right frame we have the solar angle represented by χ_3^2, as a function of the same parame-
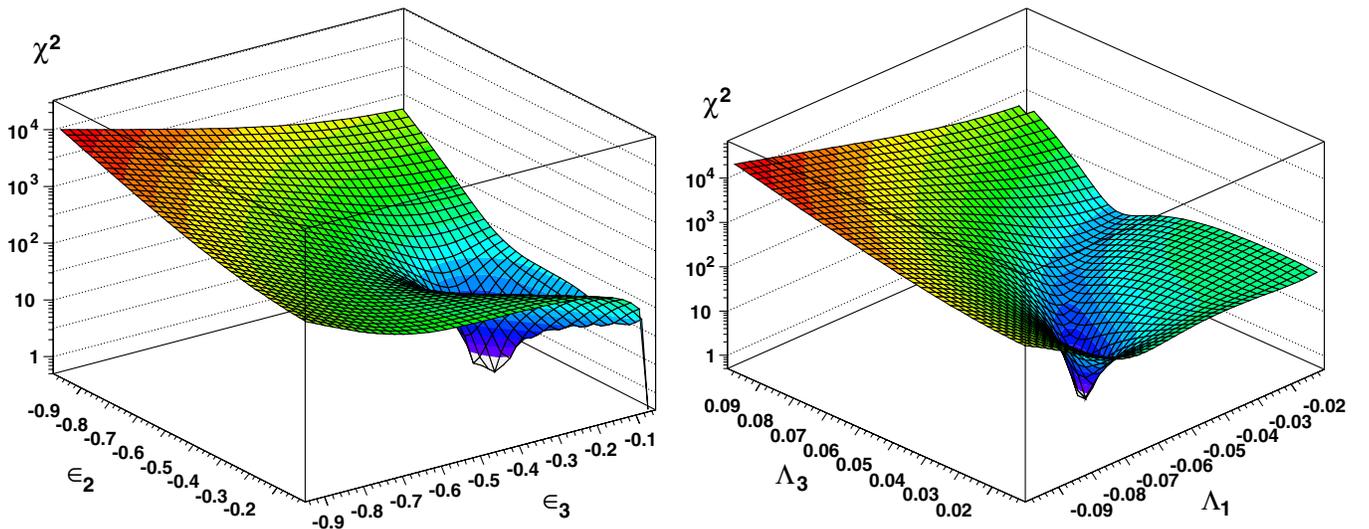
FIG. 4 (color online). χ^2 in the ϵ_2-ϵ_3 plane for the left frame and in the Λ_1-Λ_3 plane for the right frame.
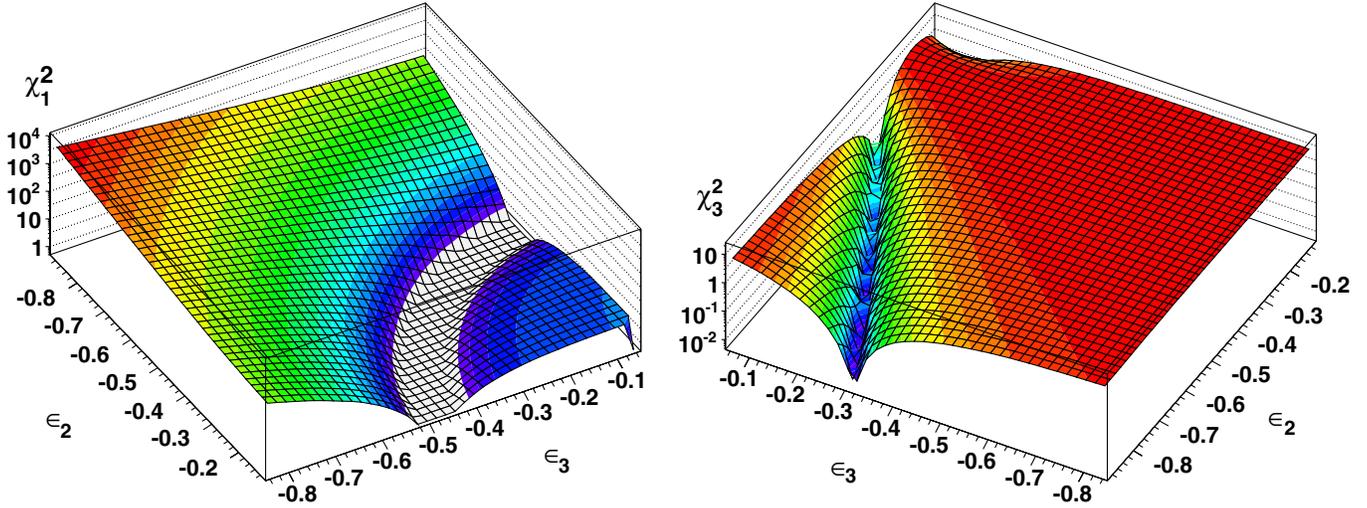
FIG. 5 (color online).   Partial χ^2 in the ϵ_2-ϵ_3 plane: atmospheric mass for the left frame, and atmospheric angle for the right frame.

ters. The behavior of χ_i^2 can be easily understood with some approximations which we develop next.

In normal circumstances the A-term dominates over the other two in Eq. (10) because it receives contributions at tree-level. Nevertheless, depending on the relative values of the ϵ_i and Λ_i parameters, it is possible for the C-term to dominate the neutrino mass matrix. This is the case with the example we are studying. We have obtained approximated solutions for eigenvalues and eigenvectors of the 3×3 effective neutrino mass matrix when the C-term is much larger than the A and B terms. In this case, the neutrino masses are,

$$
\begin{aligned}
m_3 &= C|\vec{\epsilon}|^2 + 2B(\vec{\epsilon} \cdot \vec{\Lambda}) + A\frac{(\vec{\epsilon} \cdot \vec{\Lambda})^2}{|\vec{\epsilon}|^2} \\
m_2 &= A\frac{|\vec{\epsilon} \times (\vec{\Lambda} \times \vec{\epsilon})|^2}{|\vec{\epsilon}|^4}
\end{aligned}
\tag{15}
$$

up to terms of second order, while the lightest neutrino has exactly $m_1 = 0$ when the mass matrix has the form in Eq. (10). The eigenvectors are given by the following expressions,

$$
\begin{aligned}
\vec{v}_3 &= \frac{\vec{\epsilon}}{|\vec{\epsilon}|} + \left[B + A\frac{(\vec{\epsilon} \cdot \vec{\Lambda})}{|\vec{\epsilon}|^2} \right] \frac{\vec{\epsilon} \times (\vec{\Lambda} \times \vec{\epsilon})}{C|\vec{\epsilon}|^3} \\
\vec{v}_2 &= \frac{\vec{\epsilon} \times (\vec{\Lambda} \times \vec{\epsilon})}{|\vec{\epsilon} \times (\vec{\Lambda} \times \vec{\epsilon})|} - \left[B + A\frac{\vec{\epsilon} \cdot \vec{\Lambda}}{|\vec{\epsilon}|^2} \right] \frac{|\vec{\epsilon} \times (\vec{\Lambda} \times \vec{\epsilon})|}{C|\vec{\epsilon}|^4} \vec{\epsilon} \\
\vec{v}_1 &= \frac{\vec{\Lambda} \times \vec{\epsilon}}{|\vec{\Lambda} \times \vec{\epsilon}|}
\end{aligned}
\tag{16}
$$

also up to terms of second order. Note that the eigenvectors are orthogonal and normalized up to the order we are working. The matrix U_{PMNS} is formed with the eigenvectors in its columns.

Using these approximated expressions, and neglecting Λ_2 and ϵ_1, we find,

$$
\begin{aligned}
\Delta m_{\text{atm}}^2 &= m_3^2 - m_2^2 \approx C^2(\epsilon_2^2 + \epsilon_3^2)^2 \quad \Delta m_{\text{sol}}^2 = m_2^2 - m_1^2 \\
&\approx A^2 \left[\Lambda_1^2 + \frac{\Lambda_3^2}{1 + (\epsilon_3/\epsilon_2)^2} \right]^2 \quad \tan^2\theta_{\text{atm}} = \left(\frac{v_{3,2}}{v_{3,3}}\right)^2 \\
&\approx \left(\frac{\epsilon_2}{\epsilon_3}\right)^2 \quad \tan^2\theta_{\text{sol}} = \left(\frac{v_{2,1}}{v_{3,1}}\right)^2 \approx \frac{\Lambda_1^2}{\Lambda_3^2}\left[1 + \left(\frac{\epsilon_3}{\epsilon_2}\right)^2\right].
\end{aligned}
\tag{17}
$$

With these approximations for the neutrino observables, we can easily understand the different figures. The atmospheric mass squared difference Δm_{atm}^2 in Eq. (17) indicates that constant values of this observable are obtained at circumferences in the ϵ_2-ϵ_3 plane, which is exactly what we see in the left frame of Fig. 5. At the same time, constant values of the atmospheric angle are obtained at straight lines, which is confirmed in the right frame of Fig. 5. From Eq. (17) we also see that the dependence on Λ_i of the atmospheric parameters is weak, and we do not plot it explicitly.

In Fig. 6 we concentrate on the solar neutrino parameters, and we study them as a function of Λ_1 and Λ_3. From Eq. (17) we see that the solar mass squared difference has a constant value at ellipses in the Λ_1-Λ_3 plane, and they can be seen in the left frame of Fig. 6, with the eccentricity of the ellipse depending on the ratio ϵ_3/ϵ_2. Similarly, in Eq. (17) we learn that constant values of the solar angle are obtained at straight lines in the Λ_1-Λ_3 plane, and they can be seen in the right frame of Fig. 6. The dependence of the solar observables on ϵ_i is not weak, but we do not show it here.
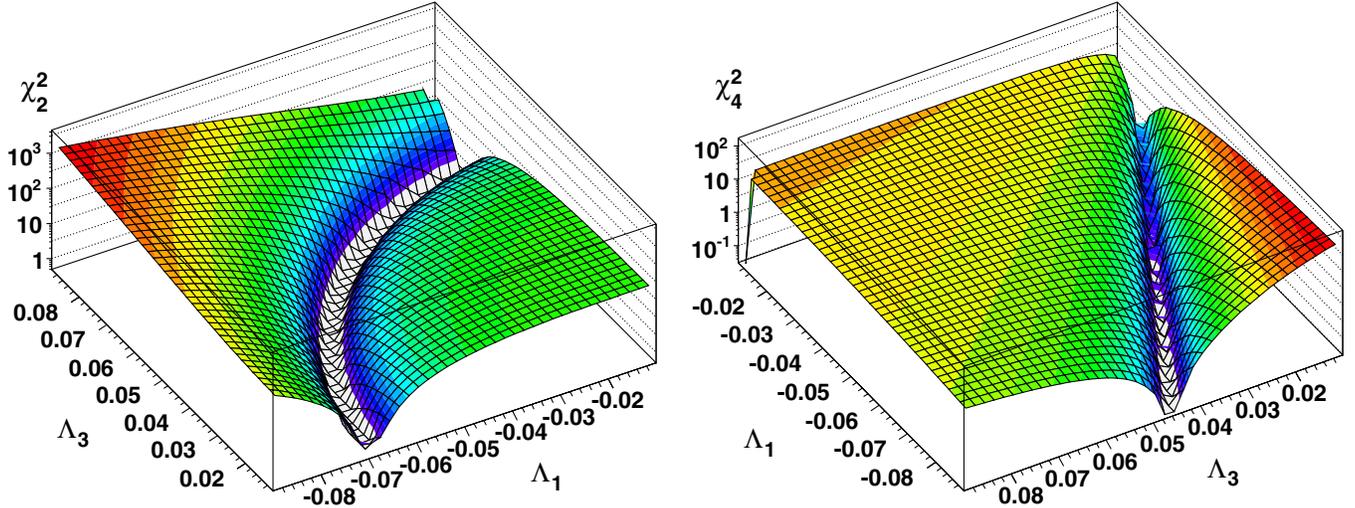
FIG. 6 (color online).   Partial χ^2 in the Λ_1-Λ_3 plane: solar mass for the left frame, and solar angle for the right frame.

C. R-parity violating decays of SUSY particles

The R-parity violating interactions are rather feeble since they are related to neutrino physics. Therefore, the R-parity violating effects are expected to be small except in processes suppressed in the R conserving scenario. In fact, the pair production of SUSY particles is nearly the same as in the case of conserved R-parity and single production of SUSY particles is strongly suppressed. The main manifestation of R-parity violation is the fact that the lightest supersymmetric particles decays.

We evaluated all possible R-parity conserving as well as R-parity violating decays for all particles. Notwithstanding, with the exception of χ_1^0 and χ_1^+ the R-parity violating channels are strongly suppressed as they are proportional to the ratios $|\vec{\epsilon}_i|^2/|\mu|^2 \simeq 10^{-6}$ and $|\vec{\Lambda}|^2/|\det(m_{\chi^0})| \simeq 10^{-8}$ and, thus, do not play any role in our analysis. Because of the near degeneracy of the lightest neutralino and chargino the decay of the latter through R-parity violating couplings is significant (often dominant) and we evaluate all RPV and RPC decay channels. The decay of χ_1^0 and χ_1^+ are calculated using the two-body decay whenever possible. Thus, for masses above the W-mass we compute the decays $\chi_1^0 \to \ell_i^\pm W^\pm$, whereas below M_W we compute the full three-body decay into all possible final states. In the three-body decays, we include all intermediates states, such as neutral scalars and pseudoscalars which can be important in some regions of parameter space [24]. However, the effects from the scalar intermediate states, except the standard model like Higgs, are less import in our AMSB model, as the scalars are fairly heavy.

The decay of the lightest neutralino in our model takes place through W, Z, neutral and charged scalar and squark states. The decays of the neutralino can be classified as leptonic ($\nu\ell\ell$), semileptonic ($\ell q\bar{q}'$, $\nu q\bar{q}$) as well as invisible ($\nu\nu\nu$). The possible BRpV chargino decay channels, induced through the same intermediate states as for

the neutralino, are $\nu q'\bar{q}$, $\ell q\bar{q}$, $\ell\ell\ell$ and $\ell\nu\nu$. Moreover, R-parity conserving chargino decays exist with the most important RPC channels being $\chi_1^+ \to \chi_1^0\pi^+$ and $\chi_1^+ \to \chi_1^0 e^+\nu$. The mass difference Δm_χ, is mainly dependent on the value of $\tan\beta$ and $m_{3/2}$, and is so small that it suppresses the RPC channel substantially. For this reason the RPC decays will have the largest branching ratio for small $m_{3/2}$ and large $\tan\beta$, since in this case Δm_χ is the largest.

To understand better the decay of these particles we plot their branching ratios in Fig. 7. The chargino decay channels with a branching ratio above 10^{-3} are plotted and for the neutralino we plot all channels above 10^{-2}. We have differentiated between bottom quarks (denoted b) and other quarks (denoted q). Also, we distinguish between a muon or an electron (commonly denoted by l) and a tau. We note, that as has already been observed [23,24] there is an important connection between the neutralino decay and the neutrino parameters. In particular, due to the large atmospheric mixing angle, an almost equal number of muons and taus is expected to be produced along with a W. This can clearly be seen from Fig. 7, as the W-mediated channels exhibit this property. We can also learn from this figure that for heavier neutralinos, i.e. larger $m_{3/2}$, the most important decay channels are μW, τW, and νZ with the νh mode having a sizeable contribution. The three-body decays grow with the increase of $m_{3/2}$, becoming important at high $m_{3/2}$ values.

The chargino branching ratios also exhibit a number of near equalities. For instance, from the right panel of Fig. 7 we can see that $BR(\chi_1^+ \to \ell Z) \simeq BR(\chi_1^+ \to \tau Z)$ as well as $BR(\chi_1^+ \to \ell h) \simeq BR(\chi_1^+ \to \tau h)$. Indeed, these equalities are found for all values of $m_{3/2}$, being a consequence of the fact that the same R-parity breaking parameters responsible for the SUSY decays govern also neutrino physics [42]. Furthermore, the chargino decays predomi-
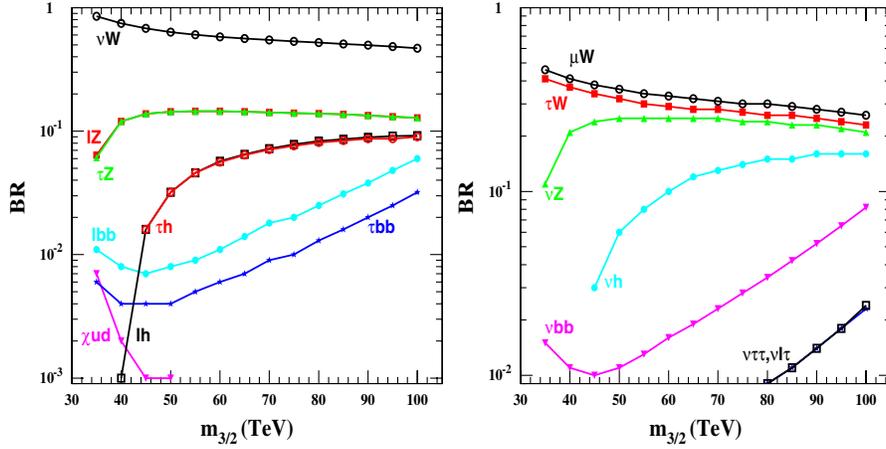
FIG. 7 (color online). The branching ratios of the lightest chargino (left) and the lightest neutralino (right) as a function of $m_{3/2}$ for $m_0 = 800$ GeV, $\tan\beta = 10$, and $\mu > 0$. We use the symbol l for an electron or a muon. By q we mean any quark not being the bottom quark, and by the ud combinations we mean any set of u-type quarks and d-type quarks. In general we sum over all states in the decay channel.

nantly into νW for all values of $m_{3/2}$ and the other important decays are ℓZ, τZ, ℓh and τh. The mass difference Δm_χ for $\tan\beta = 10$ is at most 300 MeV and as can be seen from Fig. 7, the chargino RPC branching ratios are very small and can be neglected in the analysis.

When sparticles are heavy, three-body decays of the lightest neutralino and chargino are dominated by amplitudes with intermediate gauge bosons. In this case, leptonic decays of these particles include, for example,
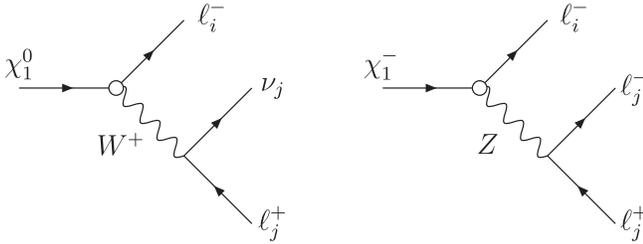
where the open circle indicates a coupling that violates R-Parity. If sparticles are not heavy, extra amplitudes with charged sleptons and sneutrinos in the intermediate state should be added, introducing more R-Parity violating couplings.

On the other hand, in the previous section we have seen that the neutrino mass matrix can be expressed in terms of the vectors $\vec{\Lambda}$ and $\vec{\epsilon}$ times coefficients depending only on R-parity conserving paramters. Neutrino data tell us that the ratios $|\Lambda|/\sqrt{\text{Det}_0}$ (or equivalently $|\Lambda|/\text{Det}_+$) and $|\vec{\epsilon}|/|\mu|$ have to be small numbers. Here Det_0 (Det_+) is the determinant of the MSSM neutralino (chargino) mass matrix. This fact can be used to expand the R-parity violating couplings in these ratios. As an example we give here the dominant $W^+ - l_i^- - \chi_1^0$ coupling:

$$O_{Li1}^{\ell nw} = \frac{g\Lambda_i}{\sqrt{2}}\left[-\frac{g'M_2\mu}{2\text{Det}_0}N_{11} + g\left(\frac{1}{\text{Det}_+} + \frac{M_1\mu}{2\text{Det}_0}\right)N_{12} \right.$$
$$- \frac{v_U}{2}\left(\frac{g^2M_1 + g'^2M_2}{2\text{Det}_0} + \frac{g^2}{\mu\text{Det}_+}\right)N_{13}$$
$$\left. + \frac{v_D(g^2M_1 + g'^2M_2)}{4\text{Det}_0}N_{14} \right] \qquad (18)$$

relevant for the neutralino decay, and the dominant $Z - l_i^- - \chi_1^+$ coupling [43]:

$$O_{R1i}^{c\ell Z} = \Lambda_i \frac{g}{2\sqrt{2}\text{Det}_+} U_{11} \qquad (19)$$

All couplings can be expanded in a similar way, with couplings involving sfermions and Higgs bosons in general having terms proportional to ϵ_i in addition to Λ_i. The complete list in case of neutralinos is given in Ref. [24]. The important point to note is, that these expansions show that the partial R-parity violating decay widths of the lightest neutralino and lightest chargino have the generic form

$$\Gamma(\tilde{\chi} \to l_i X) = \gamma_X |\alpha_X \Lambda_i + \beta_X \epsilon_i|^2 \qquad (20)$$

where γ_X describes the kinematics and α_X and β_X contain only R-parity conserving parameters. This structure remains the same if l_i is replaced by a ν_i. This feature implies that the total width, if the R-parity violating decay modes dominate, is proportional to $(a|\vec{\Lambda}|^2 + b\vec{\Lambda} \cdot \vec{\epsilon} + c|\vec{\epsilon}|^2)$ and, thus, is correlated to neutrino masses (this has been explicitly shown in Fig. 1 of the first paper in [42]).

III. COLLIDER SIGNALS

We will analyze the LHC discovery potentials for BRpV-mAMSB in various channels, that is, we study a myriad of channels, ranging from jets+missing energy to multilepton channels in addition to the displaced vertices

signal. Throughout this paper we use SPheno [34] to generate the particle spectrum and decays which are tabulated in the SLHA format [44]. The signal and background generation was carried out with PYTHIA [45] version 6.409 adopting the CTEQ5L parton distribution function [46].

A. Canonical SUSY final state topologies at LHC

We considered several canonical supersymmetry signals for the LHC, following what has been presented in Refs. [28,47]:

(1) *Inclusive jets and missing transverse momentum* (**IN**): in this class of events we include all events that present jets and missing $\not{p}_T$. In R-parity conserving scenarios this channel is one of the main search modes [28].

(2) *Zero lepton, jets and missing transverse momentum* (**0ℓ**): the events in this class present jets and missing $\not{p}_T$ without isolated leptons ($e^\pm$, $\mu^\pm$);

(3) *One lepton, jets and missing transverse momentum* (**1ℓ**): here we consider only events presenting jets and missing $\not{p}_T$ accompanied by just one isolated lepton;

(4) *Opposite sign lepton pair, jets and missing transverse momentum* (**OS**): the events in this class contain jets, missing $\not{p}_T$, and two isolated leptons of opposite charges;

(5) *Same sign lepton pair, jets and missing transverse momentum* (**SS**): here we consider only events presenting jets and missing $\not{p}_T$ accompanied by two isolated leptons of the same charge;

(6) *Multileptons, jets and missing transverse momentum* (**Mℓ**): we classify in this class the events exhibiting jets, missing $\not{p}_T$ accompanied by three or more isolated charged leptons.

In our analysis we defined jets through the subroutine PYCELL of PYTHIA with a cone size of $\Delta R = 0.7$. Charged leptons ($e^\pm$ or $\mu^\pm$) were considered isolated if the energy deposit in a cone of $\Delta R < 0.3$ is smaller than 5 GeV. Furthermore, we smeared the energies, but not directions, of all final state particles with a Gaussian error given by $\Delta E/E = 0.7/\sqrt{E}$ (E in GeV) for hadrons and $\Delta E/E = 0.15/\sqrt{E}$ for charged leptons.

We perform our event selection along the same lines of [28]. Initially, we applied the following acceptance cuts:

C1 We required at least *two* jets in the event with

$$p_T^j > 50 \text{ GeV} \quad \text{and} \quad |\eta_j| < 3. \qquad (21)$$

C2 The transverse sphericity of the event must exceed 0.2, i.e.

$$S_T > 0.2. \qquad (22)$$

This requirement reduces efficiently the large background due to the production of two jets in the SM.

C3 A potential source of missing transverse momentum in the background is the mismeasurement of jets. Therefore, we imposed the following cut in the azimuthal angle between the jets and the missing momentum ($\Delta\varphi$) to reduce the background

$$\frac{\pi}{6} \le \Delta\varphi \le \frac{\pi}{2}. \qquad (23)$$

After applying the acceptance cuts *C1–C3* we impose further cuts to each final state topology. In order to achieve some optimization of the cuts in different regions of the parameter space we used floating cuts E_T^c which can take the values 200, 300, 400, and 500 GeV. Considering that our main goal is to evaluate the impact or R-parity violation interactions on the searches for SUSY we have not tried to further improve our cuts. Given one value of E_T^c, we further required for all topologies that

$$p_T^{1,2} > E_T^c \quad \text{and} \quad \not{p}_T > E_T^c. \qquad (24)$$

where $p_T^{1,2}$ stand for the transverse momenta of the two hardest jets. These are the only additional cuts applied on the **IN** topology.

For the events in the 0ℓ class we veto the presence of isolated leptons with

$$p_T^\ell > 10 \text{ GeV} \quad \text{and} \quad |\eta_\ell| < 2.5. \qquad (25)$$

In addition to comply with (24), 1ℓ events must present only one isolated lepton satisfying

$$p_T^\ell > 20 \text{ GeV} \quad \text{and} \quad |\eta_\ell| < 2.5. \qquad (26)$$

Since the SM production of W's is a potentially large background we also imposed that the transverse mass cut

$$m_T(\not{p}_T, p_T^\ell) > 100 \text{ GeV}. \qquad (27)$$

For the **OS** (**SS**) signal we required the presence of two isolated charged leptons with opposite (same) charge after imposing (24). The hardest isolated lepton must have

$$p_T^\ell > 20 \text{ GeV} \quad \text{and} \quad |\eta_\ell| < 2.5, \qquad (28)$$

while the second lepton must satisfy (25). Multilepton events (*Mℓ*) must pass the cuts (24) and exhibit three or more isolated leptons with the hardest one satisfying (28) and the other leptons complying (25).

The most important SM backgrounds to the canonical SUSY searches are

- the process with highest cross section at small E_T^c is the QCD production $pp \rightarrow jjX$ where j denotes a jet;
- $t\bar{t}$ production that contributes to many final state topologies due to its decay into $WWbb$;
- associated production of weak bosons and jets which we denote by Wj and Zj;
- double weak boson production VV with $V = Z$ or W;
- production of a single top quark. We did not consider the gluon-W contribution to this reaction because it is not included in PYTHIA.

We present in Table I the total background cross section after cuts for the final state topologies that we analyzed. The main source of background is $t\bar{t}$ production for all the

TABLE I. Total background cross section in fb as a function of E_T^c for the channels considered here.

E_T^c/Background	IN	1ℓ	OS	SS	$M\ell$
200 GeV	261.	178.	5.4	0.40	1.3
300 GeV	24.	17.	0.32	0.013	0.001
400 GeV	4.0	3.1	0.015	0.0	0.0
500 GeV	0.88	0.63	0.003	0.0	0.0

process with Wj and Zj also contributing to the **IN** background. Moreover, Wj also plays an important role in the 1ℓ topology. For additional information on the backgrounds see Ref. [47].

Comparing our results for the SM backgrounds with the ones in Ref. [28] we can see that they agree within a factor of 2. This is indeed expected since PYTHIA and ISAJET have different choices for the event generation, specially in the hadronization procedure. This does not pose a serious problem for the LHC experiment since the backgrounds can be obtained from actual data.

B. Displaced vertices at LHC

In our BRpV-mAMSB model both χ_1^0 and χ_1^+ can travel macroscopic distances before decaying. Consequently, the long lifetimes of these particles can give rise to a further striking signal, that is, the existence of displaced vertices in the events. However, the decay must be confined within the inner parts of the detector in order for it to be fully reconstructible.

The decay lengths in the rest frame of χ_1^0 and χ_1^+ are depicted in Fig. 8 as a function of the neutralino (chargino) mass for different choices of parameters. We can see from this figure that these SUSY particles typically decay within the inner detector, even when taking into account the time dilation γ-factor. Because of the fact that the sparticles production is completely dominated by R-parity conserving interactions, there will almost always be two long-lived sparticles in the reaction chain that may lead to a displaced vertex, either χ_1^0 or χ_1^+. Thus, our analysis will require the presence of two displaced vertices in the event. Notwithstanding, there is a small corner of the parameter space where χ_1^0 and χ_1^+ decay very fast as we can see in the bottom curves of Fig. 8. This region is characterized by the LSP being the stau, and consequently, χ_1^0 and χ_1^+ fast decay is due to R-parity conserving interactions. Moreover, in this region of the parameter space the stau decay is too fast, at least by a factor of 10^4 with respect to chargino and neutralinos, washing out the displaced vertex signal.

In order to be able to see the vertex, where the chargino or neutralino decays to the secondary particles, we must require that the decay products are such that this vertex can be reconstructed. The following decay modes allow us to reconstruct the neutralino decay vertex

- $\tilde{\chi}_1^0 \rightarrow \nu \ell^+ \ell^-$ with $\ell = e$, μ denoted by $\ell\ell$;
- $\tilde{\chi}_1^0 \rightarrow \nu q\bar{q}$ denoted jj;
- $\tilde{\chi}_1^0 \rightarrow \tau q'\bar{q}$, called τjj;
- $\tilde{\chi}_1^0 \rightarrow \nu b\bar{b}$, that we denote by bb;
- $\tilde{\chi}_1^0 \rightarrow \nu \tau^+ \tau^-$, called $\tau\tau$;
- $\tilde{\chi}_1^0 \rightarrow \tau \nu \ell$, called $\tau\ell$.

Clearly, the invisible decay of the neutralino into neutrinos cannot be reconstructed and for this reason we discarded it. On the other hand, it is possible to measure the chargino decay vertex in the decays:

- $\tilde{\chi}_1^+ \rightarrow \nu q'\bar{q}$ denoted jj;
- $\tilde{\chi}_1^+ \rightarrow \tau^+ q\bar{q}$, called τjj;
- $\tilde{\chi}_1^+ \rightarrow \tau^+ b\bar{b}$, called τbb;
- $\tilde{\chi}_1^+ \rightarrow \tau^+ \ell^+ \ell^-$, called $\tau\ell\ell$;
- $\tilde{\chi}_1^+ \rightarrow \ell^+ b\bar{b}$, that we denote by ℓbb;
- $\tilde{\chi}_1^+ \rightarrow \ell^+ \ell^+ \ell^-$, that we denote by $\ell\ell\ell$;
- $\tilde{\chi}_1^+ \rightarrow \ell^+ q\bar{q}$, that we denote by ℓjj.

Although the decay $\tilde{\chi}_1^+ \rightarrow \nu\nu\ell^+$ can give rise to a $e^\pm$ or $\mu^\pm$ with a high impact parameter, we do not consider the
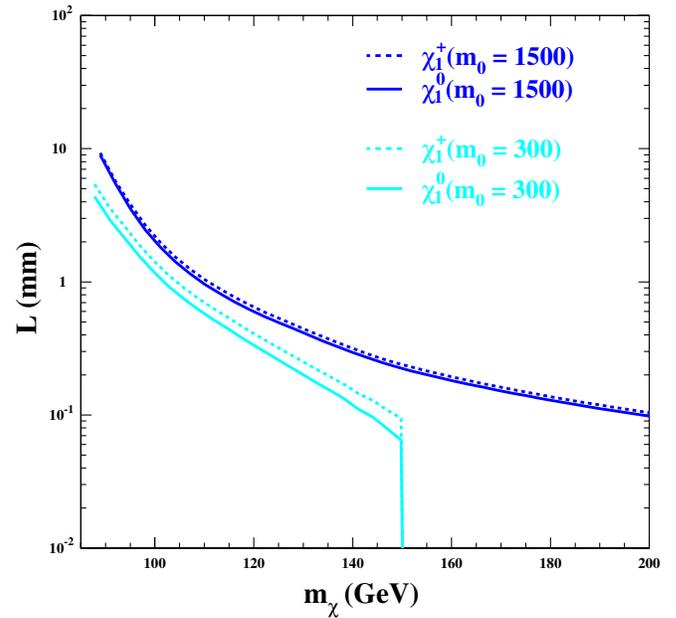

FIG. 8 (color online). The decay length in the rest frame of the lightest neutralino and the lightest chargino as a function of the mass for $\tan\beta = 10$ and $\mu > 0$.

mode in our study since it is not possible to obtain its decay vertex.

We considered a crude model of the LHC detectors in order to identify events containing displaced vertices. We selected events presenting neutralino or chargino decays away from the primary vertex via the requirement that the displaced neutralino/chargino vertex is outside an ellipsoid around the primary vertex

$$\left(\frac{x}{\delta_{xy}}\right)^2 + \left(\frac{y}{\delta_{xy}}\right)^2 + \left(\frac{z}{\delta_z}\right)^2 = 1,$$

where the z-axis is along the beam direction. We took $\delta_{xy} = 100\ \mu$m and $\delta_z = 2.5$ mm that correspond to 5 times the expected resolution in each direction. To guarantee a high efficiency in the reconstruction of the displaced vertices without a full detector simulation, we required the tracks leaving the displaced vertex to be inside the rapidity coverage of the vertex detector, i.e. $|\eta| < 2.5$. Moreover, we also required that the displaced vertices are inside the vertex detector—that is, the vertices must be within a radius of 550 mm and z-axis length of 800 mm.

The SM backgrounds coming, for instance, from displaced vertices associated to b's or τ's can be eliminated by requiring that the tracks defining a displaced vertex should have an invariant mass larger than 20 GeV. This way the displaced vertex signal passing all the above cuts is essentially physics background free, however, there might exist instrumental backgrounds which were not considered here.

An important issue in the displaced vertex search is the trigger on the events containing them. In order to mimic the triggers used by the LHC collaborations, we accept events passing at least one of the following requirements:

- The event has one isolated electron with $p_T > 20$ GeV;
- The event has one isolated muon with $p_T > 6$ GeV;
- The event has two isolated electrons with $p_T > 15$ GeV;
- The event has one jet with $p_T > 100$ GeV;
- The event has missing transversal energy >100 GeV.

IV. DISCOVERY REACH AT THE LHC

We estimated the LHC discovery reach in all the channels described in Sec. III A. We required that either the signal leads to 5σ departure from the background where this is not vanishing or 5 events in regions where there is no SM background. We present our results in the $m_{3/2} \otimes m_0$ plane for $\tan\beta = 10$, $\mu > 0$ and integrated luminosities of 10 fb^{-1} and 100 fb^{-1}.

We depict in Fig. 9 the LHC discovery potential in the all inclusive channel (**IN**). For the sake of comparison, we also present in this figure the discovery reach assuming R-parity conservation. As we can see from this figure, the introduction of bilinear R-parity violation reduces the reach in $m_{3/2}$ for a given value of m_0 if we use the search strategy design for the R-parity conserving case. Basically, the decay of the LSP reduces the missing transverse energy making it harder to disentangle the SUSY signal and the SM background. Comparing the left and right panels of Fig. 9, we can see that a larger luminosity in this channel expands the reach in $m_{3/2}$ from $\simeq 70$–80 TeV to $\simeq$90–100 TeV.

The reach in the 1ℓ channel is presented in Fig. 10. In the R-parity conserving scenario this channel is sensitive to the spectrum details of mAMSB since the lightest chargino decay contains soft charged particles in addition to the LSP and consequently, there are less channels available that give rise to hard leptons. Once again the introduction of R-parity violation depletes this signal because of the re-
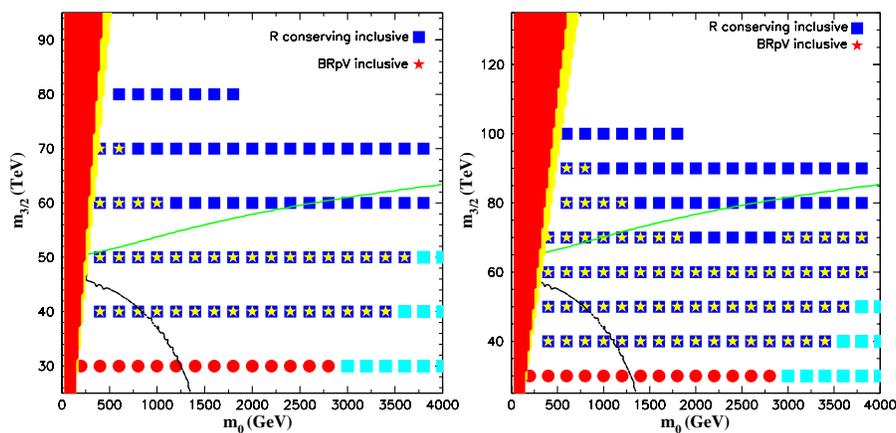

FIG. 9 (color online).   Discovery reach in the inclusive channel (**IN**) for $\tan\beta = 10$, $\mu > 0$ and the integrated luminosities of 10 fb^{-1} (left panel) and 100 fb^{-1} (right panel). The dark (blue) square mark the points where mAMSB with R-parity conservation can be discovered while the stars stand for the reach of our BRpV-mAMSB model. Dark (red) circles stand for the points excluded by LEP data while no solution for the neutrino masses was found in the gray (cyan) squares. The dark (red) area on the left is theoretically excluded by the existence of tachyonic particles and the light shaded area adjacent to this one is the area with a stau LSP. The light (green) line is the contour for the gluino mass of 1 TeV. The Higgs mass is 114 GeV on the dashed dark line.
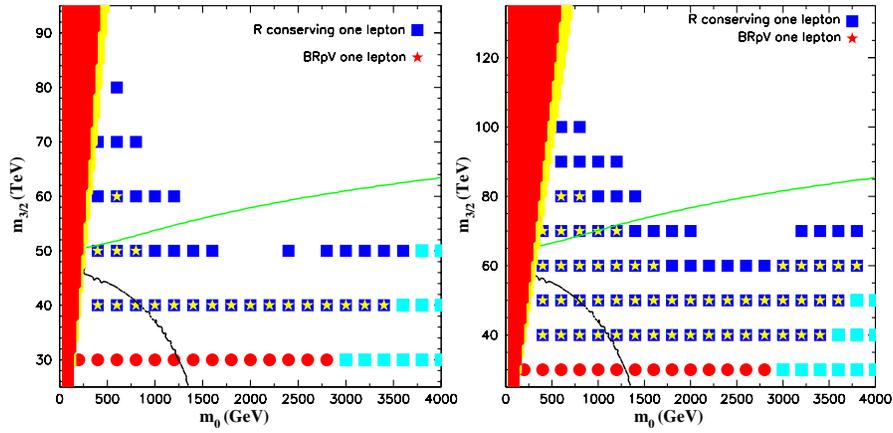
FIG. 10 (color online).   Discovery reach in the one lepton channel for the parameters and conventions used in Fig. 9.
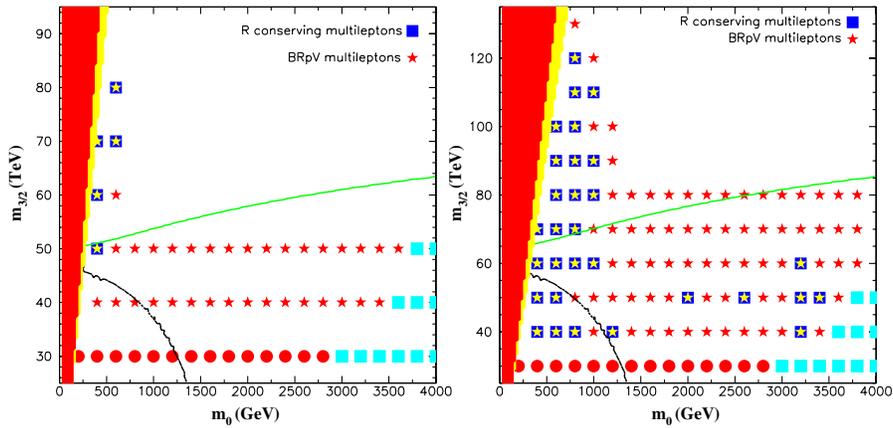

FIG. 11 (color online).   Discovery reach in the multilepton channel for the parameters and conventions used in Fig. 9.
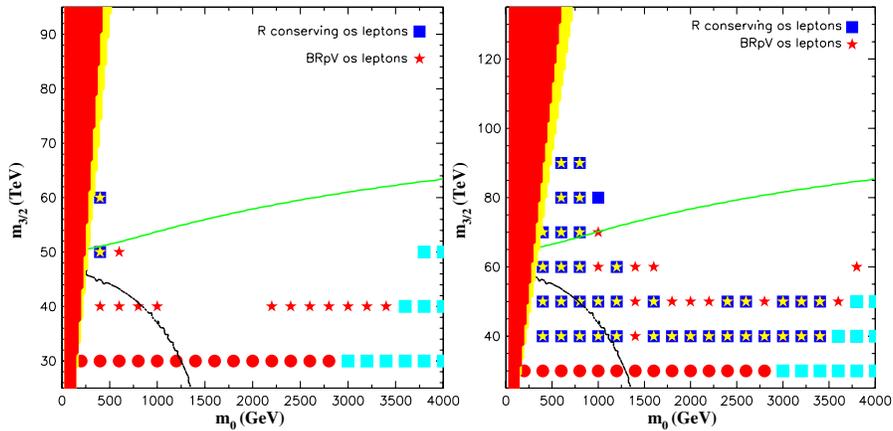

FIG. 12 (color online).   Discovery reach in the opposite sign lepton channel for the parameters and conventions used in Fig. 9.
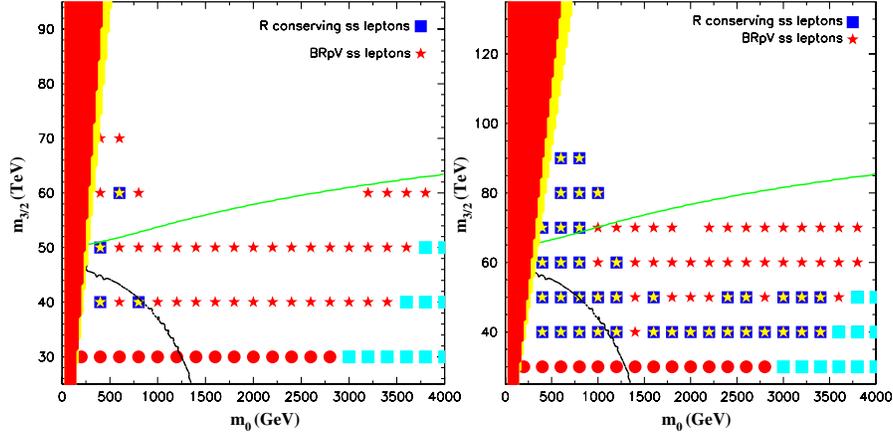
FIG. 13 (color online).   Discovery reach in the same sign lepton channel for the parameters and conventions used in Fig. 9.

duced missing transverse momentum. Moreover, the extra produced leptons in the chargino or neutralino decays have the tendency of contributing to the trilepton topology. Comparing the left ad right panels of this figure it is clear that the reach in this channel is extended with the increase of the luminosity, however, its reach is still smaller than the **IN** one.

The reach in the multilepton channel is depicted in Fig. 11. For 10 fb^{-1} the R-parity conserving scenario has a very limited reach with the signal being sizeable only in the area presenting light sleptons. The inclusion of BRpV interactions increases the LHC reach in the **Mℓ** channel at small values of $m_{3/2}$ with the **IN** and **Mℓ** having similar reaches at low luminosities. At higher luminosities, 100 fb^{-1}, the multilepton channel reach is considerably extended with and without R-parity conservation, being this the channel with largest reach at small m_0. Moreover, this is the SUSY canonical topology with the largest potential for discovery in the R-parity violating scenario.

We also studied the exclusive channels containing two isolated charged leptons verifying that the introduction of R-parity violating interactions enhances these channels. In the R-parity violating scenario the LHC **OS** reach is similar to the **1ℓ** channel one except at large m_0 where the **OS** signal has a reduced reach; see Fig. 12. On the other hand, the **SS** channel presents a smaller SM background in addition to an enhanced signal due to the presence of majorana states in SUSY models. Therefore, this topology has a good discovery reach in our BRpV-mAMSB model as can be seen from Fig. 13. In fact, the **SS** final state has a slightly larger reach than the fully inclusive mode **IN**, with the **SS** channel being the second most important channel in the presence of BRpV interactions.

Before we move on to the displaced vertex signal, we would like to stress that our results are an indication of R-parity violating interactions in the canonical SUSY searches. Certainly, the introduction of a larger number of floating cuts leads to larger reaches in all channels, like the ones in Ref. [29]. Nevertheless, the depletion of the

fully inclusive channel and the enhancement of exclusive topologies containing isolated leptons, as compared to the R-conserving case, must persist in a more elaborate analysis. In this light, it should be possible to determine whether R-parity is broken or not by combining the results of all the canonical SUSY search channels.

The smoking gun of BRpV-mAMSB is the existence of detached vertices exhibiting a high invariant mass. There is no SM background for these events except for possible instrumental backgrounds, rendering this channel a very strong evidence for Physics beyond the standard model. We present in Fig. 14 the reach in the displaced vertex topology for integrated luminosities of 10 and 100 fb^{-1}.
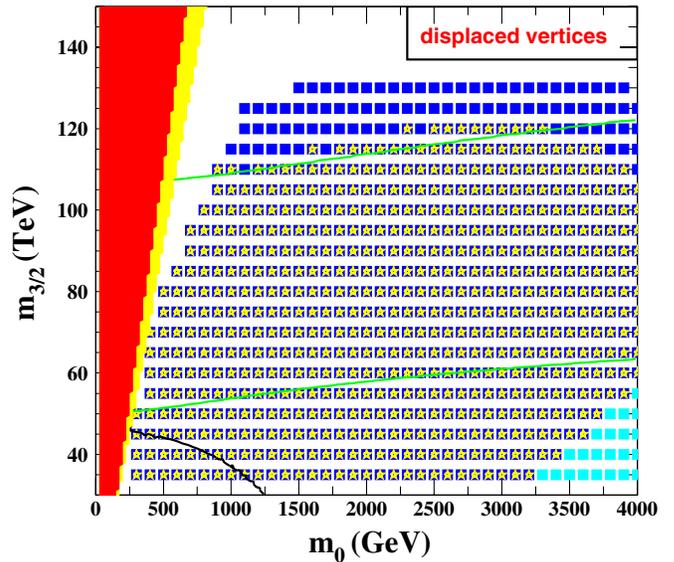

FIG. 14 (color online).   Discovery reach for the LHC in displaced vertices channel for $\tan\beta = 10$ and $\mu > 0$ in the $m_{3/2} \otimes m_0$ plane and an integrated luminosities of 10 fb^{-1} (stars) and 100 fb^{-1} [dark (blue) squares]. The light (green) lines gives the contour of a gluino mass of 1 TeV and 2 TeV. All other conventions follow the ones of Fig. 9.

As we can see from this figure, this channel does have the largest reach ($\simeq 110(120)$ TeV for $10(100)$ fb^{-1}) with the nice feature of being almost independent of m_0, except at small m_0 where the presence of light scalars lead to rapid neutralino and chargino decay; see Fig. 8.

V. CONCLUSIONS

We have studied the phenomenology of AMSB model augmented with bilinear R-parity parameters at the LHC. We show that the presence of bilinear R-parity interactions modifies the canonical channels used for the supersymmetry search. The decay of the neutralino and chargino weaken the fully inclusive signal, however, the existence of further leptons in the final state leads to an enhancement of the leptonic exclusive modes. In the case that the BRpV-mAMSB final state contains three or more charged leptons the reach is so enhanced that this channel alone has a comparable reach to the fully inclusive one with R-parity conservation. One interesting aspect of the drastic change in the reach of the different topologies is that a possible positive signal at the LHC can be used to disentangle models with and without R-parity conservation.

Our BRpV-mAMSB model connects the R-parity violating parameters to measured neutrino properties. Because of the smallness of the couplings needed to reproduce the observed neutrino masses and mixings, our model predicts a rather large lifetime for charginos and neutralinos. This leads to the smoking gun of the BRpV-mAMSB theory, that is, the existence of displaced vertices associated to neutralino or chargino decays that exhibit a large visible invariant mass. We showed that the search for such detached vertices does lead to the largest discovery reach for such models. Indeed this channel can probe $m_{3/2}$ up to $\simeq$ 100 TeV, which constitutes almost all the natural parameter space. At this point it is interesting to point out that the search of detached vertices at the Tevatron can cover a large fraction of the presently allowed parameter space. We depict in Fig. 15 the parameter space region that can be probed at the Tevatron for an integrated luminosity of 2 fb^{-1}, showing that the Tevatron collaborations can al-
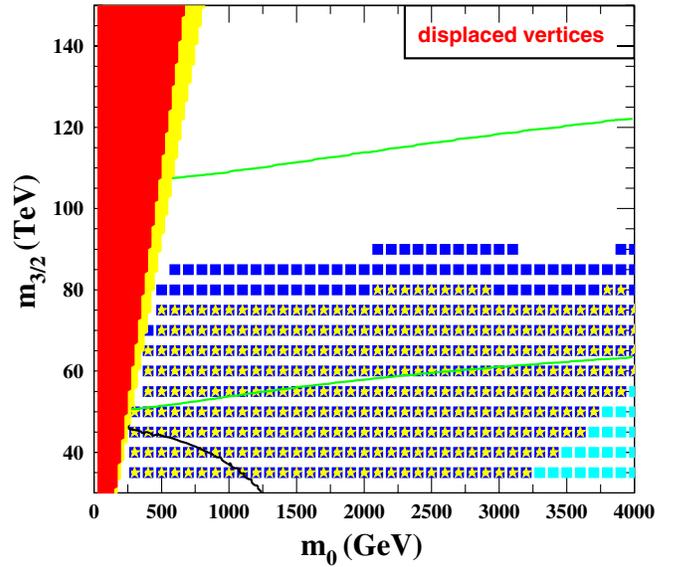

FIG. 15 (color online). Discovery reach at the Tevatron in displaced vertices channel for $\tan\beta = 10$, $\mu > 0$ in the $m_{3/2} \otimes m_0$ plane and an integrated luminosity of 2 fb^{-1} (stars) and 10 fb^{-1} [dark (blue) squares]. The light (green) lines gives the contour of a gluino mass of 1 TeV and 2 TeV. All other conventions follow the ones of Fig. 9.

ready cover a lot of ground in searching for BRpV-mAMSB.

ACKNOWLEDGMENTS

[1] Y. Y. Ashie *et al.* (Super-Kamiokande Collaboration), Phys. Rev. D **71**, 112005 (2005).

[2] B. T. Cleveland *et al.*, Astrophys. J. **496**, 505 (1998); C. Cattadori, Results from Radiochemical Solar Neutrino Experiments, Talk Given at XXIst International Conference on Neutrino Physics and Astrophysics (NU2004), Paris, 2004; W. Hampel *et al.* (GALLEX Collaboration), Phys. Lett. B **447**, 127 (1999); S. Fukuda *et al.* (Super-Kamiokande Collaboration), Phys. Rev. Lett. **86**, 5651 (2001); Q. R. Ahmad *et al.* (SNO Collaboration), Phys.

Rev. Lett. **87**, 071301 (2001); **89**, 011302 (2002); S. N. Ahmed *et al.* (SNO Collaboration), Phys. Rev. Lett. **92**, 181301 (2004); S. B. Aharmim *et al.* (SNO Collaboration), Phys. Rev. C **72**, 055502 (2005).

[3] T. Araki *et al.* (KamLAND Collaboration), Phys. Rev. Lett. **94**, 081801 (2005); K. Eguchi *et al.* (KamLAND Collaboration), Phys. Rev. Lett. **90**, 021802 (2003); S. Abe *et al.* (KamLAND Collaboration), arXiv:0801.4589.

[4] E. Aliu *et al.* (K2K Collaboration), Phys. Rev. Lett. **94**, 081802 (2005).

[5] N. Tagg (MINOS Collaboration), *Proc. 4th Flavor Physics and CP Violation Conference (Vancouver)*, eConf C060409, 019 (2006).

[6] M. Apolloni *et al.* (CHOOZ Collaboration), Phys. Lett. B **420**, 397 (1998); Eur. Phys. J. C **27**, 331 (2003).

[7] D. N. Spergel *et al.*, Astrophys. J. Suppl. Ser. **170**, 377 (2007).

[8] M. Gell-Mann, P. Ramond, and R. Slansky, in *Supergravity*, edited by P. van Niewenhuizen and D. Freedman (North-Holland, Amsterdam, 1979); T. Yanagida, in *Prodeedings of the Workshop on Unified Theroy and Baryon Number in the Universe*, edited by Sawada and A. Sugamoto (KEK, Thuhuba, 1979), Report No 79–18. R. N. Mohapatra and G. Senjanovic, Phys. Rev. Lett. **44**, 912 (1980); J. Schechter and J. W. F. Valle, Phys. Rev. D **22**, 2227 (1980).

[9] A. Freitas, W. Porod, and P. M. Zerwas, Phys. Rev. D **72**, 115002 (2005).

[10] A. Zee, Phys. Lett. **93B**, 389 (1980); **95B**, 461(E) (1980); C. Jarlskog, M. Matsuda, S. Skadhauge, and M. Tanimoto, Phys. Lett. B **449**, 240 (1999); K. R. S. Balaji, W. Grimus, and T. Schwetz, Phys. Lett. B **508**, 301 (2001).

[11] K. S. Babu, Phys. Lett. B **203**, 132 (1988).

[12] D. Aristizabal Sierra and D. Restrepo, J. High Energy Phys. 08 (2006) 036.

[13] D. Aristizabal Sierra and M. Hirsch, J. High Energy Phys. 12 (2006) 052.

[14] For a review, see R. Barbier *et al.*, Phys. Rep. **420**, 1 (2005).

[15] L. J. Hall and M. Suzuki, Nucl. Phys. **B231**, 419 (1984); J. R. Ellis, G. Gelmini, C. Jarlskog, G. G. Ross, and J. W. F. Valle, Phys. Lett. B **150B**, 142 (1985); R. Hempfling, Nucl. Phys. **B478**, 3 (1996); E. Nardi, Phys. Rev. D **55**, 5772 (1997).

[16] D. E. Kaplan and A. E. Nelson, J. High Energy Phys. 01 (2000) 033; C. H. Chang and T. F. Feng, Eur. Phys. J. C **12**, 137 (2000).

[17] M. Hirsch, M. A. Diaz, W. Porod, J. C. Romao, and J. W. F. Valle, Phys. Rev. D **62**, 113008 (2000); **65**, 119901(E) (2002); M. A. Diaz, M. Hirsch, W. Porod, J. C. Romao, and J. W. F. Valle, Phys. Rev. D **68**, 013009 (2003); **71**, 059904(E) (2005); D. W. Jung, S. K. Kang, J. D. Park, and E. J. Chun, J. High Energy Phys. 08 (2004) 017; E. J. Chun, S. K. Kang, C. W. Kim, and U. W. Lee, Nucl. Phys. **B544**, 89 (1999).

[18] A. Santamaria and J. W. F. Valle, Phys. Lett. B **195**, 423 (1987); J. C. Romao and J. W. F. Valle, Nucl. Phys. **B381**, 87 (1992); H. P. Nilles and N. Polonsky, Nucl. Phys. **B484**, 33 (1997); R. Kitano and K. y. Oda, Phys. Rev. D **61**, 113001 (2000).

[19] G. F. Giudice, M. A. Luty, H. Murayama, and R. Rattazzi, J. High Energy Phys. 12 (1998) 027.

[20] L. Randall and R. Sundrum, Nucl. Phys. **B557**, 79 (1999).

[21] F. De Campos, M. A. Diaz, O. J. P. Eboli, M. B. Magro, and P. G. Mercadante, Nucl. Phys. **B623**, 47 (2002).

[22] F. de Campos, M. A. Diaz, O. J. P. Eboli, R. A. Lineros, M. B. Magro, and P. G. Mercadante, Phys. Rev. D **71**, 055008 (2005).

[23] B. Mukhopadhyaya, S. Roy, and F. Vissani, Phys. Lett. B **443**, 191 (1998).

[24] W. Porod, M. Hirsch, J. Romao, and J. W. F. Valle, Phys. Rev. D **63**, 115004 (2001).

[25] F. de Campos, O. J. P. Eboli, M. B. Magro, W. Porod, D. Restrepo, and J. W. F. Valle, Phys. Rev. D **71**, 075001 (2005).

[26] V. D. Barger, T. Han, S. Hesselbach, and D. Marfatia, Phys. Lett. B **538**, 346 (2002).

[27] M. B. Magro, F. de Campos, O. J. P. Eboli, W. Porod, D. Restrepo, and J. W. F. Valle, J. High Energy Phys. 09 (2003) 071.

[28] H. Baer, J. K. Mizukoshi, and X. Tata, Phys. Lett. B **488**, 367 (2000).

[29] A. J. Barr, C. G. Lester, M. A. Parker, B. C. Allanach, and P. Richardson, J. High Energy Phys. 03 (2003) 045.

[30] S. Roy, Mod. Phys. Lett. A **19**, 83 (2004).

[31] B. C. Allanach and A. Dedes, J. High Energy Phys. 06 (2000) 017.

[32] T. Gherghetta, G. F. Giudice, and J. D. Wells, Nucl. Phys. **B559**, 27 (1999).

[33] H. K. Dreiner, C. Luhn, and M. Thormeier, Phys. Rev. D **73**, 075007 (2006).

[34] W. Porod, Comput. Phys. Commun. **153**, 275 (2003).

[35] B. C. Allanach, A. Dedes, and H. K. Dreiner, Phys. Rev. D **60**, 056002 (1999).

[36] W. M. Yao *et al.*, J. Phys. G **33**, 1 (2006).

[37] V. M. Abazov *et al.* (D0 Collaboration), Phys. Lett. B **638**, 119 (2006).

[38] A. Dedes, S. Heinemeyer, S. Su, and G. Weiglein, Nucl. Phys. **B674**, 271 (2003).

[39] K. Hagiwara, A. D. Martin, D. Nomura, and T. Teubner, Phys. Lett. B **649**, 173 (2007); M. Davier, S. Eidelman, A. Hocker, and Z. Zhang, Eur. Phys. J. C **31**, 503 (2003).

[40] A. L. Kagan and M. Neubert, Eur. Phys. J. C **7**, 5 (1999); G. Degrassi, P. Gambino, and G. F. Giudice, J. High Energy Phys. 12 (2000) 009; M. Carena, D. Garcia, U. Nierste, and C. E. M. Wagner, Phys. Lett. B **499**, 141 (2001); T. Hurth, E. Lunghi, and W. Porod, Eur. Phys. J. C **33**, S382 (2004); G. Degrassi, P. Gambino, and P. Slavich, Phys. Lett. B **635**, 335 (2006); M. E. Gomez, T. Ibrahim, P. Nath, and S. Skadhauge, Phys. Rev. D **74**, 015015 (2006).

[41] M. Maltoni, T. Schwetz, M. A. Tortola, and J. W. F. Valle, New J. Phys. **6**, 122 (2004).

[42] M. Hirsch and W. Porod, Phys. Rev. D **68**, 115007 (2003); M. Hirsch, W. Porod, J. C. Romao, and J. W. F. Valle, Phys. Rev. D **66**, 095006 (2002).

[43] A. G. Akeroyd, M. A. Diaz, and J. W. F. Valle, Phys. Lett. B **441**, 224 (1998).

[44] P. Skands, J. High Energy Phys. 07 (2004) 036.

[45] T. Sjostrand, Comput. Phys. Commun. **82**, 74 (1994); T. Sjostrand, P. Eden, C. Friberg, L. Lonnblad, G. Miu, S. Mrenna, and E. Norrbin, Comput. Phys. Commun. **135**, 238 (2001).

[46] H. L. Lai *et al.* (CTEQ Collaboration), Eur. Phys. J. C **12**, 375 (2000).

[47] F. de Campos, O. J. P. Eboli, M. B. Magro, W. Porod, D. Restrepo, M. Hirsch, and J. W. F. Valle, J. High Energy Phys. 05 (2008) 048.